

Stabilization of Blue Emitters with Thermally Activated Delayed Fluorescence by the Steric Effect: A Case Study by means of Magnetic Field Effects

Chongguang Zhao^{1,*}, Fenggui Zhao^{2,**}, Kai Wang^{1,†}, Haomiao Yu^{2,‡}, Tianyu Huang¹, Rui Wang¹, Caixia Zhang², Bin Hu^{3,‡}, and Lian Duan^{1,4,§}

¹Key Lab of Organic Optoelectronics and Molecular Engineering of Ministry of Education, Department of Chemistry, Tsinghua University, Beijing 100084, People's Republic of China

²Key Laboratory of Luminescence and Optical Information, Ministry of Education, School of Science, Beijing Jiaotong University, Beijing 100044, People's Republic of China

³Joint Institute for Advanced Materials, Department of Materials Science and Engineering, University of Tennessee, Knoxville, Tennessee 37996, USA

⁴Center for Flexible Electronics Technology, Tsinghua University, Beijing 100084, People's Republic of China

(Received 15 May 2020; revised 24 August 2020; accepted 25 August 2020; published 23 September 2020)

The use of steric hindrance in blue thermally activated delayed fluorophores shows empirically the improvement of operational lifetime for organic light-emitting diodes (OLEDs). Nevertheless, the intrinsic mechanism of this strategy remains unclear and elusive. Here, the steric effects on rate coefficient and degradation probability of bimolecular quenching processes are decoupled by magnetic field effects and quantum-chemical calculation. The respective dependence of magnetoelectroluminescence on triplet density and charge-carrier density indicates that triplet-charge quenching (TCQ) is the dominant degradation mechanism over that of triplet-triplet annihilation, where steric hindrance effectively prevents the occurrence of Dexter-type TCQ and significantly reduces the TCQ rate coefficient. On the contrary, only a slight increase in degradation probability is generated by the steric effect from bulk inert groups. These findings will provide unambiguous guidance for the design of functional materials for OLEDs.

DOI: 10.1103/PhysRevApplied.14.034059

I. INTRODUCTION

Thermally activated delayed fluorescence (TADF) provides an upward conversion pathway for the efficient utilization of normally nonemissive triplet excited states. Since employment in organic light-emitting diodes (OLEDs) [1], it has progressively boosted the internal quantum efficiencies of electroluminescence (EL) toward an upper limit. However, the severe degradation of blue TADF devices during operation still prevents their commercialization in white lighting and large-area displays. In addition to impacts from extrinsic factors, such as moisture, oxygen, and impurities, which can be solved by advanced manufacturing technologies, there is more one can do from academic point of view to gain a deeper understanding of the intrinsic degradation mechanisms, and therefore, to propose theoretical strategies for operational lifetime elongation.

It is widely expected that exciton-charge interactions and exciton-exciton interactions are the main degradation mechanisms, and particularly, exciton-charge quenching (ECQ) dominates for electrically stressed diodes [2,3]. In the ECQ degradation model, the rate of molecular degradation can be described as

$$r_{\text{degr,ECQ}} = p_{\text{degr,ECQ}} k_{\text{ECQ}} n_{\text{ext}} n_c , \quad (1)$$

where n_{ext} and n_c are the density of exciton and charge, respectively; k_{ECQ} is the rate coefficient of ECQ; and $p_{\text{degr,ECQ}}$ is the degradation probability of each ECQ process [4]. In terms of the manipulation of density and distribution of exciton and charge carrier, we demonstrate a significantly extended lifetime through expediting both reverse intersystem crossing (RISC) of the host and Förster energy transfer between host and dye, and utilizing shallow dye trap-assisted charge transport [5]. However, in spite of this, the strategies for degradation alleviation from inhibiting k_{ECQ} and $p_{\text{degr,ECQ}}$ are also worth investigation. For this idea, molecular design should be a feasible approach.

We report a series of sky-blue TADF emitters with electron-donating carbazolyl groups and an electron-accepting cyano group [6]. Molecules with steric hindrance from *tert*-butyl groups show distinctly higher

*kaiwang@bjtu.edu.cn

†yuhaomiao@bjtu.edu.cn

‡bhu@utk.edu

§duanl@mail.tsinghua.edu.cn

**These authors contributed equally to this work.

stability than that of their counterparts without such groups. After device optimization, a favorable half-lifetime of 269 h is achieved in an OLED based on 2,3,4,5,6-pentakis-(3,6-di-*tert*-butyl-9*H*-carbazol-9-yl)benzonitrile (5TCzBN) under an initial luminance of 1000 cd m⁻² [7]. However, it is still unclear how steric effects alleviate degradation and stabilize the diode's operation. The lack of physical chemistry insights still limits this strategy on giving explicit guidance for device architecture design.

Here, using TADF emitters 5TCzBN and 2,3,4,5,6-penta-(9*H*-carbazol-9-yl)benzonitrile (5CzBN) as samples, the effects of the steric groups on reducing the in-device degradation rate are decoupled by the nondestructive magnetic-field-effect (MFE) technique and quantum-chemical computations. Through this approach, the mechanism of device stabilization from steric effects is intrinsically elucidated.

II. MECHANISM AND METHODS

The magnetic field can be utilized as a tool to disturb the spin statistics in the organic semiconductor; the internal spin-related light-emitting property can be revealed in terms of magnetooelectroluminescence (MEL) and magnetophotocurrent (MPC). The magnitude of MFE for a signal S is calculated by

$$E_{MF,S} = \frac{S(B) - S(0)}{S(0)} , \quad (2)$$

where $S(B)$ and $S(0)$ are the signals with and without the field B , respectively [8]. ECQ includes singlet-charge quenching and triplet-charge quenching (TCQ), where TCQ constitutes the plausible degradation mechanisms along with triplet-triplet annihilation (TTA). At lower magnetic fields (usually less than 50 mT), MEL originates from the perturbation of spin statistics at charge-transfer (CT) states, and the intersystem crossing (ISC) is mainly governed by the hyperfine fields and spin-orbit coupling. When ISC is dominant over RISC, the ratio of the CT singlet state [¹(CT)] to the CT triplet [³(CT)] can be increased by the magnetic field, leading to positive MPC and positive MEL, due to the replenishing of more easily dissociative and radiative singlets [9]. Alternatively, negative MPC and negative MEL would result when RISC were the dominant process. At higher magnetic fields, as both TTA and TCQ provide spin-conversion pathways [TTA: ($\uparrow\uparrow$) + ($\uparrow\uparrow$) \rightarrow ($\uparrow\downarrow$) or ($\uparrow\uparrow$) + ($\downarrow\downarrow$) \rightarrow ($\uparrow\downarrow$), TCQ: ($\uparrow\uparrow$) + \downarrow \rightarrow ($\uparrow\downarrow$) + \uparrow] [10], the impediment of TTA or TCQ from Zeeman splitting effect would invoke a negative MEL [11]. In particular, a negative MPC can be caused by higher magnetic fields at the existence of apparent ECQ. Since part of the ECQ process activates trapped charges at the tail of their density of state to free carriers ($E + e/h \rightarrow S_0 + e/h^*$, where E is a singlet or triplet

exciton; S_0 is the singlet ground state; e and h represent an electron and a hole, respectively; and “*” indicates an excited state), the inhibition of ECQ by higher magnetic fields would thereby result in a negative MPC [12].

Since the kinetics of TTA and TCQ can be, respectively, expressed as

$$r_{TTA} = k_{TTA} n_T^2 , \quad (3)$$

$$r_{TCQ} = k_{TCQ} n_T n_c , \quad (4)$$

where r_{TTA} , r_{TCQ} , k_{TTA} , and k_{TCQ} denote rates and rate coefficients of TTA and TCQ, respectively. n_T is the triplet density. The gradient of MEL amplitude with respect to n_T (i.e., $|dMEL/dn_T|$) and n_c (i.e., $|dMEL/dn_c|$) at identical magnetic field intensities can reflect k_{TTA} and k_{TCQ} in a dedicated emissive layer (EML), respectively. Analogously, the rate coefficient of the same interaction in different material systems can be compared by their respective gradients of MEL amplitude. Therefore, the factors of rate coefficient and degradation probability in Eq. (1) can be decoupled by the MFE measurements and quantum-chemical computations. Herein, a useful and reliable method to manipulate n_T is to adjust the current densities in charge-balanced devices [13]. While the manipulation of n_c requires the blocking of one type of charge carrier during charge injection, the other type is collected by preventing it from flowing out [14].

III. RESULTS AND DISCUSSION

A. Devices and their electrical properties

Devices with the structure of ITO/MoO₃(10 nm)/5TCzBN or 5CzBN(12 mol %):3,3-di(9*H*-carbazol-9-yl) biphenyl mCBP (60 nm)/4,7-diphenyl-1,10-phenanthroline (BPhen)(10 nm)/*n*-C₂₄F₅₀(x nm)/LiF(1 nm)/Al(120 nm) are designed and fabricated for MFE measurements. The energy diagram of the devices and chemical structures of the materials are given in Figs. 1(a) and 1(b), respectively, with 5TCzBN and 5CzBN doped in mCBP as the EML; LiF and MoO₃ as the electron-injection layer (EIL) and hole-injection layer (HIL), respectively; and BPhen as the electron-transport layer (ETL). An insulating straight-chain perfluoroalkane interlayer, perfluorotetracosane (*n*-C₂₄F₅₀), is introduced between the EIL and ETL to break the in-device electron-hole balance and build a hole-rich EML [15]. According to quantum-chemical calculations, the highest occupied molecular orbital (HOMO) and lowest unoccupied molecular orbital (LUMO) levels of *n*-C₂₄F₅₀ are -10.27 and -2.25 eV, respectively, ensuring its good insulating properties [16].

The current-density–voltage (j - V) characteristics of 5TCzBN and 5CzBN devices with various insulating layer (IL) thicknesses are shown in Figs. 1(c) and 1(d), respectively. An interesting phenomenon of electron-injection

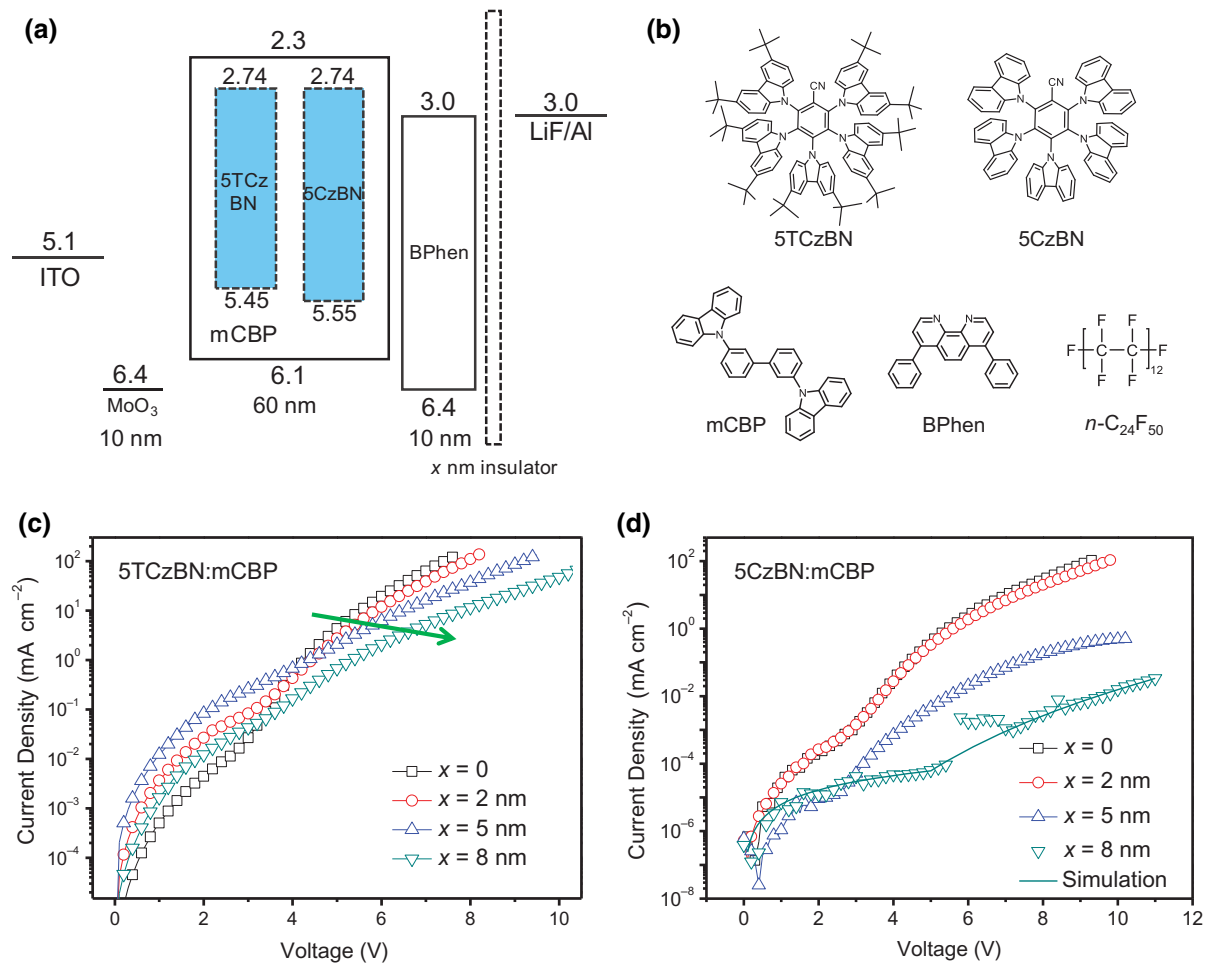


FIG. 1. (a) Energy diagram of studied devices, (b) chemical structure of organic materials, and j - V characteristics of (c) 5TCzBN:mCBP and (d) 5CzBN:mCBP devices at various insulating-layer thicknesses (x): 0 (black), 2 nm (red), 5 nm (blue), 8 nm (dark cyan). Solid line of 5CzBN:mCBP device with x = 8 nm denotes the simulated j - V curves, according to space-charge-limited current model (Fig. S3e within the Supplemental Material [17]).

improvement is found in the 5TCzBN device with an IL thickness (x) below 5 nm [Fig. 1(c) under 3 V], which then decreases at 8 nm insulator condition. This will be discussed in detail in our subsequent article. Nonetheless, the voltage always increases with increasing x at a higher current density (over 1 mA cm⁻²), which is applied in the following MFE measurements, showing the inferior conductivity of n -C₂₄F₅₀. This also causes almost inverse correlations of the external quantum efficiency (EQE) and luminance at identical voltages with x (Figs. S1 and S2 within the Supplemental Material [17]). Notably, the 5CzBN device with x = 5 nm only exhibits a maximum j of 0.5 mA cm⁻² [Fig. 1(d)] and maximum luminance of 24.5 cd m⁻² (Fig. S2d within the Supplemental Material [17]), while 5TCzBN devices can work normally, even with x = 17 nm (Fig. S1 within the Supplemental Material [17]); this indicates that the ability of 5TCzBN molecules to withstand a high density of positive charges, much higher than that of 5CzBN molecules.

B. Magnetic-field-effect study

The MPC of the charge-balanced 5TCzBN device (without IL) is measured to investigate whether there is an obvious ECQ effect. The distinct current at zero voltage under sunlight irradiation shows adequate charge separation in the 5TCzBN:mCBP blend (Fig. S3a within the Supplemental Material [17]). A semiconductor laser of 405 nm wavelength and 100 mW cm⁻² power intensity is selected to generate the photocurrent (Fig. S3b within the Supplemental Material [17]). From the obtained MPC of the 5TCzBN device (x = 0) in Fig. 2, at lower magnetic fields, the photocurrent increases sharply with an increase of magnetic field intensity, whereas, after the magnetic field exceeds 60 mT, the downward MPC trend with an increase of the external magnetic field emerges. Since the ¹(CT) to ³(CT) ratio is field dependent and can be easily manipulated, the positive MPC at lower magnetic fields is attributed to the increase of the ¹(CT) to ³(CT) ratio by

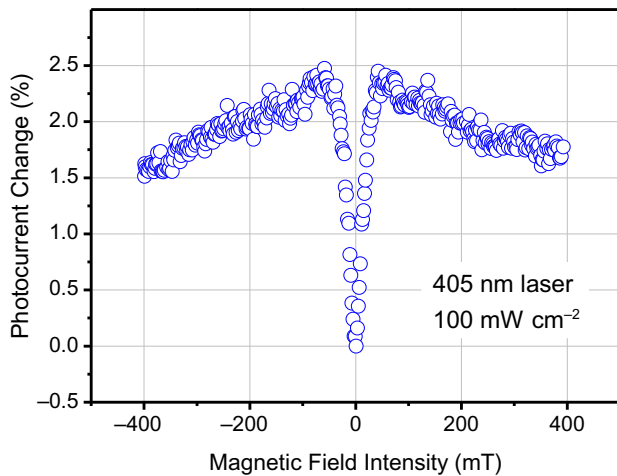


FIG. 2. Obtained magnetophotocurrent of charge-balanced 5TCzBN device (without insulating layer) at 405 nm, 100 mW cm^{-2} laser excitation.

affecting the spin states of polaron pairs [Fig. 3(a)] and the larger dissociation tendency of $^1(\text{CT})$ [12]. Nevertheless, the apparent in-device ECQ process should take responsibility for the negative MPC under a higher magnetic field; the activation of trapped charge is inhibited by the impeded ECQ.

Moreover, the MEL of 5TCzBN and 5CzBN devices with various x and at various applied current densities is measured to understand the predominant degradation mechanism and steric effect on the bimolecular interactions of TTA and TCQ. From the current-density dependence of the MEL of the 5TCzBN device [Fig. 3(b)], the ascendant MEL at lower magnetic fields originates from the increased $^1(\text{CT})$ to $^3(\text{CT})$ ratio, corresponding to the MPC result. At higher magnetic fields, the inverse correlation of MEL versus current density does not appear and, instead, there is a slight upward trend, showing that TTA is not significant [13,18]. However, the in-device hole carrier density has a notable effect on the MEL in the charge-unbalanced device. From the MEL of the 5TCzBN device with various x at an identical current density of 50 mA cm^{-2} , the MEL decreases intensely as the IL thickness increases [Fig. 3(c)], indicating the strong interaction of the spin-conversion TCQ process [Fig. 3(a)] [11]. The MEL at $x = 11 \text{ nm}$ reaches an amplitude of 15.1%. The IL-thickness-dependent MEL is also measured at identical current densities of 20 and 100 mA cm^{-2} (Fig. S4 within the Supplemental Material [17]). Although with different absolute amplitudes, the MEL under these current-density criteria shows almost the same IL thickness dependence.

For the 5CzBN device, the current-density dependence of the MEL shows almost the same tendency and amplitude as that of the 5TCzBN device at lower magnetic fields [Fig. 3(d)], while the distinct negative MEL appears at higher magnetic fields ($>60 \text{ mT}$), representing the higher

TTA reactivity of 5CzBN than that of 5TCzBN. The charge-unbalanced device of 5CzBN shows a rather large negative MEL, with an amplitude of 28.8% at 800 mT , even when the IL thickness is only 2 nm [Fig. 3(e)], and 5CzBN devices with IL thicknesses above 2 nm fail to meet the current-density and luminance requirements for MEL testing. Compared with the maximum amplitude of the negative MEL caused by TTA of only 2.4%, TCQ in the 5CzBN matrix is also demonstrated to be a stronger interaction than that of TTA. The MEL of the 5CzBN device at a current density of 20 mA cm^{-2} also exhibits a compatible IL-thickness dependence (Fig. S5 within the Supplemental Material [17]). Therefore, it is reasonable to believe that TCQ is the primary mechanism of molecular degradation of both blue fluorophores based on both reasons of (i) its stronger interaction than that of TTA and (ii) the higher probability for the heterolytic cleavage of fragile polar bonds in an excited ionic radical (charge carrier) than that of the homolytic cleavage of a neutral exciton [2].

From the above findings, it is important to further explore the steric effect on TCQ reactivity. Because n_c in a dedicated EML structure is positively correlated with x , k_{TCQ} can be reflected by $|d\text{MEL}/dx|$ [11]. The MEL amplitude versus x of 5TCzBN and 5CzBN devices is extracted from Figs. 3(c) and 3(e), respectively, and depicted in Fig. 4. Here, the MEL amplitudes are averaged by the weight of magnetic field intensity to eliminate accidental errors. An interesting phenomenon is that the MEL exhibits a linear correlation with x , making $d\text{MEL}/dx$ almost a constant, which is worth more in-depth investigation. Obviously, the MEL- x correlation of the 5CzBN device is much steeper than that of the 5TCzBN device, where $|d\text{MEL}/dx|$ of the 5CzBN device ($12.78\% \text{ nm}^{-1}$) is 10 times that of the 5TCzBN device ($1.28\% \text{ nm}^{-1}$). This shows clearly that k_{TCQ} in the 5TCzBN film is significantly suppressed by steric hindrance compared with that in the 5CzBN film, which can apparently alleviate the overall degradation rate, according to Eq. (1).

TCQ includes both those of Förster-type and Dexter-type. In the model of a central exciton capturing the diffusional charge, the steady-state effective rate coefficient of Dexter-type TCQ ($k_{\text{TCQ,eff}}$) is given by

$$k_{\text{TCQ,eff}} = 4\pi DR_{c,\text{eff}} \quad (5)$$

and is affected by both the effective capture radius ($R_{c,\text{eff}}$) of the exciton and the diffusion coefficient of the charge (D), where $R_{c,\text{eff}}$ varies within a wide range of larger than 1 nm under realistic conditions [19]. In the 5TCzBN:mCBP and 5CzBN:mCBP systems, both the exciton and charge reside on the dye molecules because of their lower triplet energy and lower transport energy for electrons and holes. Based on the typical 1-nm site spacing in the simulation of an amorphous organic film [20,21], the average distance between the 12 mol % doped dye molecules is calculated

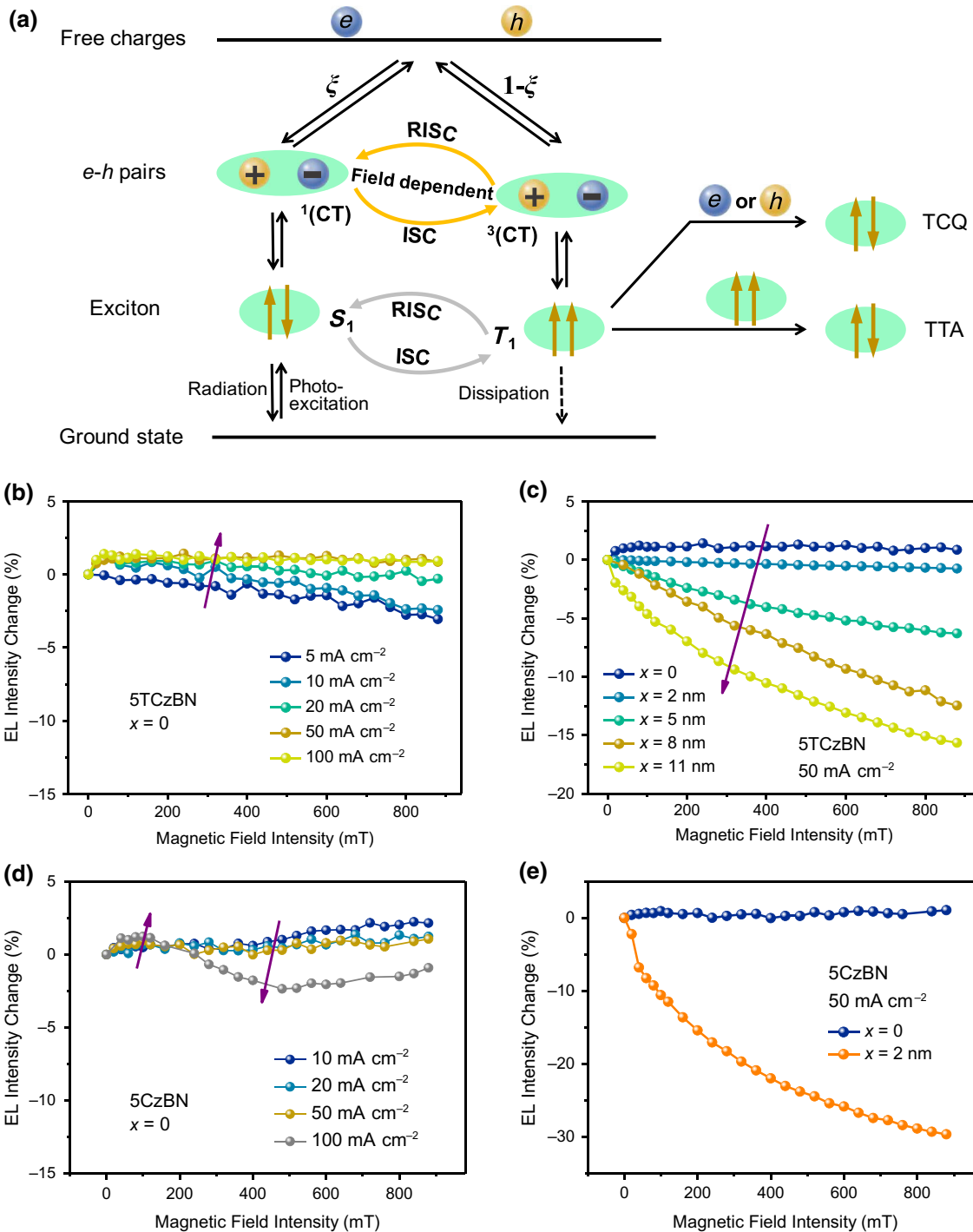


FIG. 3. (a) Diagram of charge recombination and exciton dissociation process, where ξ is the spin fraction, and the obtained magnetooptoluminescence of (b),(c) 5TCzBN device and (d),(e) 5CzBN device: (b), (d) for various current densities without an insulating layer and (c),(e) for various insulating layer thicknesses (x) at an identical current density of 50 mA cm^{-2} .

to be 2.0 nm. Therefore, on one hand, the introduction of bulk inert groups increases the molecular radius, which is equivalent to a reduction in $R_{c,\text{eff}}$ of the central triplet exciton. On the other hand, the increase in molecular size also mitigates charge diffusion, resulting in a smaller D [22]. The combined effects of steric hindrance on the triplet

and the charge effectively block the Dexter-type TCQ and reduce the overall k_{TCQ} .

C. Quantum-chemical calculations

In addition to k_{TCQ} , the rate of TCQ-caused diode aging also depends on the degradation probability of

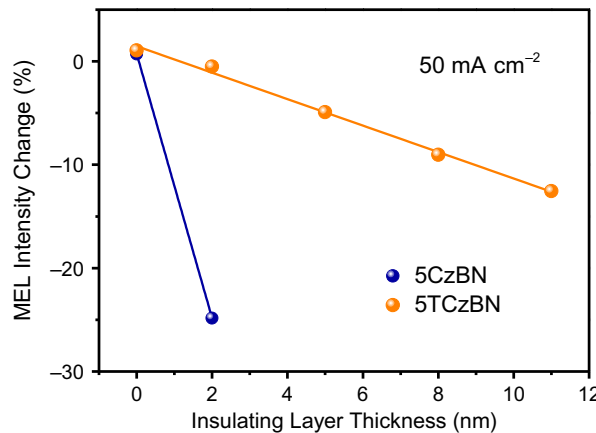


FIG. 4. MEL amplitude versus insulating-layer thickness for 5TCzBN device and 5CzBN device at an identical current density of 50 mA cm^{-2} .

each TCQ process, $p_{\text{degr,TCQ}}$, which is typically in the range of $(0.01\text{--}1) \times 10^{-8}$ [2,4]. Here, the steric effect on the degradation probability is analyzed through quantum-chemical calculations. According to the rules reported by Wang *et al.* in the donor- π structure [23], for substituents on the π side, the dissociation energy of the fragile C—N bond (BDE_f) almost solely inversely correlates with the steric hindrance of the *ortho* groups. Thus, the fragile C—N bonds in 5CzBN and 5TCzBN molecules are located at the *para* position of the cyano group. Since the heterolytic cleavage of an ionic radical is the primary degradation mechanism, the BDE_f of the above C—N bonds in the cation and anion radicals are calculated in Gaussian 09 software using density-functional theory with the B3LYP functional and 6-31G(d) basis set, as listed in Table I. The calculated BDE_f values of both anion radicals are smaller than those of the cation radicals, indicating quenching between triplets and electrons is likely to possess a higher degradation probability. Notably, although the introduction of bulky *tert*-butyl groups decreases the BDE_f of both the cation and anion radicals, which coincides with the effect of electron-donating groups on the 3,6-positions of the donor side given by Wang *et al.* [23], the change of BDE_f is still small (<0.1 eV), and the overall degradation rate is still restricted by the drastically

decreased k_{TCQ} . The general effect of steric hindrance is thereby to alleviate diode aging.

IV. CONCLUSION

The steric effect on the degradation of blue TADF molecules is investigated. The rate coefficient and degradation probability are decoupled by the respective study of the magnetic field effects and quantum-chemical calculations to understand the change in overall degradation rate. The magnetophotocurrent of the 5TCzBN device shows distinct exciton-charge quenching. The respective dependence of the magnetoelectroluminescence on the triplet density and charge-carrier density shows that TCQ is the primary degradation mechanism over TTA. Steric hindrance from the bulky inert groups effectively blocks the Dexter-type TCQ by the combined reduction of the triplet-capture radius and charge-diffusion coefficient, resulting in a drastically decreased TCQ rate coefficient, which is verified by the gradient of the MEL versus charge density for the 5CzBN and 5TCzBN cases. Quantum-chemical calculations show that steric hindrance from the bulky *tert*-butyl groups in 5TCzBN only slightly decreases the bond dissociation energy of the fragile C—N bond and increases the degradation probability. Therefore, the mechanism for device-degradation alleviation by steric effects is to inhibit the rate coefficient of TCQ. As charge accumulation (and thereby the TCQ process) mainly appears near the EML/ETL interface [24,25], apart from application in dye molecules, the additional employment of bulky groups in the molecular design of hole-blocking materials may further optimize the diode stability without intensely impeding electron transport (compared with that employed in the EML). This may provide inspiration for the selection of materials in device-architecture design.

ACKNOWLEDGMENTS

This work is supported by the National Basic Research Program of China (Grants No. 2016YFB0401003 and No. 2017YFA0204501), the National Natural Science Fund of China (Grants No. 61634001, No. U1601651, No.

TABLE I. Calculated BDE_f of each bond dissociation reaction.

Species	Bond dissociation reaction ^a	BDE_f^b (eV)
Cation radical	$5\text{CzBN}^{\bullet+} \rightarrow [5\text{CzBN} - p\text{Cz}]^+ + \text{Cz}^\bullet$	3.76
	$5\text{TCzBN}^{\bullet+} \rightarrow [5\text{TCzBN} - p\text{TCz}]^+ + \text{TCz}^\bullet$	3.67
Anion radical	$5\text{CzBN}^{\bullet-} \rightarrow [5\text{CzBN} - p\text{Cz}]^\bullet + \text{Cz}^-$	2.55
	$5\text{TCzBN}^{\bullet-} \rightarrow [5\text{TCzBN} - p\text{TCz}]^\bullet + \text{TCz}^-$	2.49

^a $p\text{Cz}$ and $p\text{TCz}$ represent the *para*-carbazole group in 5CzBN and *para*-3,6-di-*tert*-butylcarbazole group in 5TCzBN, respectively.

^bCalculated at the B3LYP/6-31G(d) level.

61974010, and No. 61904011), the Foshan Xianhu Laboratory of Advanced Energy Science and Technology, Guangdong Laboratory (Grant. No. XHT 2020-005).

-
- [1] A. Endo, K. Sato, K. Yoshimura, T. Kai, A. Kawada, H. Miyazaki, and C. Adachi, Efficient up-conversion of triplet excitons into a singlet state and its application for organic light emitting diodes, *Appl. Phys. Lett.* **98**, 083302 (2011).
 - [2] C. Zhao and L. Duan, Review on photo- and electrical aging mechanisms for neutral excitons and ions in organic light-emitting diodes, *J. Mater. Chem. C* **8**, 803 (2020).
 - [3] Q. Niu, R. Rohloff, G. A. H. Wetzelaeer, P. W. M. Blom, and N. I. Craciun, Hole trap formation in polymer light-emitting diodes under current stress, *Nat. Mater.* **17**, 557 (2018).
 - [4] R. Coehoorn, H. van Eersel, P. Bobbert, and R. Janssen, Kinetic Monte Carlo study of the sensitivity of OLED efficiency and lifetime to materials parameters, *Adv. Funct. Mater.* **25**, 2024 (2015).
 - [5] C. Zhao, C. Li, Y. Li, Y. Qiu, and L. Duan, Understanding the operational lifetime expansion methods of thermally activated delayed fluorescence sensitized OLEDs: A combined study of charge trapping and exciton dynamics, *Mater. Chem. Front.* **3**, 1181 (2019).
 - [6] D. Zhang, M. Cai, Y. Zhang, D. Zhang, and L. Duan, Sterically shielded blue thermally activated delayed fluorescence emitters with improved efficiency and stability, *Mater. Horiz.* **3**, 145 (2016).
 - [7] M. Cai, D. Zhang, J. Xu, X. Hong, C. Zhao, X. Song, Y. Qiu, H. Kaji, and L. Duan, Unveiling the role of Langevin and trap-assisted recombination in long lifespan OLEDs employing thermally activated delayed fluorophores, *ACS Appl. Mater. Interfaces* **11**, 1096 (2019).
 - [8] H. Xu, M. Wang, Z.-G. Yu, K. Wang, and B. Hu, Magnetic field effects on excited states, charge transport, and electrical polarization in organic semiconductors in spin and orbital regimes, *Adv. Phys.* **68**, 49 (2019).
 - [9] Q. Peng, A. Li, Y. Fan, P. Chen, and F. Li, Studying the influence of triplet deactivation on the singlet-triplet interconversion in intra-molecular charge-transfer fluorescence-based OLEDs by magneto-electroluminescence, *J. Mater. Chem. C* **2**, 6264 (2014).
 - [10] A. Obolda, Q. Peng, C. He, T. Zhang, J. Ren, H. Ma, Z. Shuai, and F. Li, Triplet-polaron-interaction-induced upconversion from triplet to singlet: A possible way to obtain highly efficient OLEDs, *Adv. Mater.* **28**, 4740 (2016).
 - [11] M. Shao, L. Yan, M. Li, I. Ilia, and B. Hu, Triplet-charge annihilation versus triplet-triplet annihilation in organic semiconductors, *J. Mater. Chem. C* **1**, 1330 (2013).
 - [12] F. Zhao, K. Wang, J. Duan, X. Zhu, K. Lu, C. Zhao, C. Zhang, H. Yu, and B. Hu, Spin-dependent electron-hole recombination and dissociation in nonfullerene acceptor ITIC-based organic photovoltaic systems, *Solar RRL* **3**, 1900063 (2019).
 - [13] P. Yuan, X. Qiao, D. Yan, and D. Ma, Magnetic field effects on the quenching of triplet excitons in exciplex-based organic light emitting diodes, *J. Mater. Chem. C* **6**, 5721 (2018).
 - [14] N. Chitranningrum, T.-Y. Chu, P.-T. Huang, T.-C. Wen, and T.-F. Guo, Modulating the line shape of magnetoconductance by varying the charge injection in polymer light-emitting diodes, *AIP Adv.* **8**, 025209 (2018).
 - [15] D. Yokoyama, K.-I. Nakayama, T. Otani, and J. Kido, Wide-range refractive index control of organic semiconductor films toward advanced optical design of organic optoelectronic devices, *Adv. Mater.* **24**, 6368 (2012).
 - [16] T. Takada, H. Kikuchi, H. Miyake, Y. Tanaka, M. Yoshida, and Y. Hayase, Determination of charge-trapping sites in saturated and aromatic polymers by quantum chemical calculation, *IEEE Trans. Dielectr. Electr. Insul.* **22**, 1240 (2015).
 - [17] See the Supplemental Material at <http://link.aps.org/supplemental/10.1103/PhysRevApplied.14.034059> for details of the experimental methods, optoelectronic properties of devices, selection of the photocurrent-generation conditions, and the MEL at other current density conditions.
 - [18] M. Tanaka, R. Nagata, H. Nakanotani, and C. Adachi, Understanding degradation of organic light-emitting diodes from magnetic field effects, *Commun. Mater.* **1**, 18 (2020).
 - [19] R. Coehoorn, L. Zhang, P. A. Bobbert, and H. van Eersel, Effect of polaron diffusion on exciton-polaron quenching in disordered organic semiconductors, *Phys. Rev. B* **95**, 134202 (2017).
 - [20] H. Li and J.-L. Brédas, Quasi-one-dimensional charge transport can lead to nonlinear current characteristics in organic field-effect transistors, *J. Phys. Chem. Lett.* **9**, 6550 (2018).
 - [21] C. Zhao, C. Li, and L. Duan, A competitive hopping model for carrier transport in disordered organic semiconductors, *Phys. Chem. Chem. Phys.* **21**, 9905 (2019).
 - [22] D. P. Valencia and F. J. González, Understanding the linear correlation between diffusion coefficient and molecular weight. A model to estimate diffusion coefficients in acetonitrile solutions, *Electrochim. Commun.* **13**, 129 (2011).
 - [23] R. Wang, Y.-L. Wang, N. Lin, R. Zhang, L. Duan, and J. Qiao, Effects of ortho-linkages on the molecular stability of organic light-emitting diode materials, *Chem. Mater.* **30**, 8771 (2018).
 - [24] D. Y. Kondakov, J. R. Sandifer, C. W. Tang, and R. H. Young, Nonradiative recombination centers and electrical aging of organic light-emitting diodes: Direct connection between accumulation of trapped charge and luminance loss, *J. Appl. Phys.* **93**, 1108 (2003).
 - [25] S. Nowy, W. Ren, A. Elschner, W. Lövenich, and W. Brüting, Impedance spectroscopy as a probe for the degradation of organic light-emitting diodes, *J. Appl. Phys.* **107**, 054501 (2010).